journal

J. Am. Ceram. Soc., 99 [1] 152–157 (2016)
DOI: 10.1111/jace.13924

Potential Barrier of (Zn,Nb)SnO_2-Films Induced by Microwave Thermal Diffusion of Cr^{3+} for Low-Voltage Varistor

Glauco M. M. M. Lustosa,[‡,†] João Paulo de Campos da Costa,[§] Leinig A. Perazolli,[‡] Biljana D. Stojanovic,[¶] and Maria Aparecida Zaghete[‡]

[‡]Instituto de Química - UNESP, Araraquara, São Paulo, Brazil

[§]Centro Universitário de Araraquara - UNIARA, Araraquara, São Paulo, Brazil

[¶]Institute for Multidisciplinary Research University of Belgrade, Belgrade, Serbia

The effect of Cr^{3+} on the electrical properties of SnO_2-based films deposited by electrophoresis on Si/Pt substrate was considered. The films were sintered in a microwave oven at 1000°C/40 min and then the surface was modified with deposition of Cr^{3+} ions by electrophoresis. The diffusion of Cr^{3+} contributes to the modification of the potential barrier formed on the grain boundary improving the electrical properties due to electron acceptor species adsorption on the grain boundary. The influence on the properties of grain boundary was verified by *I* versus *V* characterization in as a function of temperature. The films showed nonlinear coefficient over 9, potential barrier height over 0.5 eV and resistivity greater than 10^7 Ω·cm. 4 samples were prepared at same conditions and presented similar electrical behavior, showing the efficiency of technique on reproducibility to varistor properties control. Thereby the nonlinear coefficient increases while decreasing the conductivity of the system is noticed.

I. Introduction

The SnO_2-based ceramics application such as varistors of high or low voltage is directly linked to height and width of the potential barrier formed in the grain-boundaries region, which can be controlled by sintering or by the amount of metal present in the region.[1–4] The efficiency of varistor is determined by the nonlinear coefficient α, representing the electrical response of the material in relation to disagree of Ohm's law. This nonlinear coefficient α can be calculated by Eq. (1).

$$a = (\log E_2 - \log E_1)^{-1} \quad (1)$$

where E_2 is the electric field when current density is 10 mA/cm^2 and E_1 being the electric field when current density is 1 mA/cm^2.[5,6]

The origin of potential barrier has been investigated by some authors in an attempt to explain the mechanisms responsible for the electrical characteristics of the varistor ceramics based on SnO_2. It is known that the potential barrier existing in the grain-boundary region is dependent on the additives (amount and type of defects induced by them) and proportional to the nominal voltage of a varistor.[5,7–10] The potential barrier is formed by SnO_2 intrinsic defects (V''_{Sn}, V''_O) as well by extrinsic defects created by the addition of modifying agents, as shown in Eqs. (2–4).[11]

$$ZnO \xrightarrow{SnO_2} Zn'' + V_O^{\bullet\bullet} + O_O^X \quad (2)$$

$$2Nb_2O_5 \xrightarrow{SnO_2} 4Nb_{Sn}^{\bullet\bullet} + V''_{Sn} + 10O_o^x \quad (3)$$

$$Cr_2O_3 \xrightarrow{SnO_2} 2Cr'_{Sn} + V_O^{\bullet\bullet} + 3O_O^X \quad (4)$$

The positive donors ($V_O^{\bullet\bullet}$, $Nb_{Sn}^{\bullet}$) have a charge density (N_d) on both sides of the grain boundary forming a positive interface (depletion layer) of width *d*. The negative interface is formed during the sintering process and is composed of the acceptors donors (V''''_{Sn}, V''_{Sn}, M''_{Sn}, O′, O′) with density surface states (N_S) at the interfaces of the grain boundaries. These defects are responsible for the formation of a double barrier for the electrical transport between the grains of SnO_2 in the grain-boundary region.[12–14]

As noted in the literature,[11,15–17], the increase in the electrical properties is dependent of addition of chromium in the systems. The nonlinear coefficient (α) has a significant improvement and this is related to increase in potential barrier height, since it provides greater blocking the transport of electric current. It was reported that chromium segregated at the grain-boundary region and modifies the barrier potential and promote the resistivity for potential barrier model proposed by Bueno et al.[18]

The superficial addition of Cr^{3+} ions on varistor and further thermal treatment allow the diffusion of these ions into the samples leading to a direct modification of the grain-boundary region and resulting in an improvement of the electrical properties, as well a decreasing of sintering temperature. The purpose of this research was to verify the influence of chromium on electrical properties at grain boundary of surface on SnO_2-based films aiming to use it as low voltage varistors.

II. Experimental Procedure

(1) Reagents

Tin (II) chloride dehydrate (Synth, Diadema/SP, Brazil), zinc oxide (Unimauá, Mauá/SP, Brazil), niobium pentoxide (CBMM, Tokyo, Japan), ethyleneglycol (Synth) and citric acid (Merck, Darmstadt, Germany). Ammonia solution (Quemis, Indaiatuba/SP, Brazil), silver nitrate (Merck), nitric acid (Quemis), hydrofluoric acid (Synth), calcium carbonate (Merck) and distilled water were the other reagents used. All reagents had analytical purity.

(2) Ceramic Powder Preparation

Figure 1 resumes the preparation of polymeric solutions by the Pechini method, which immobilizes the metal ion in a

J. Varela—contributing editor

Manuscript No. 36437. Received February 17, 2015; approved August 2, 2015.
†Author to whom correspondence should be addressed. e-mail: glauco.morandi@gmail.com

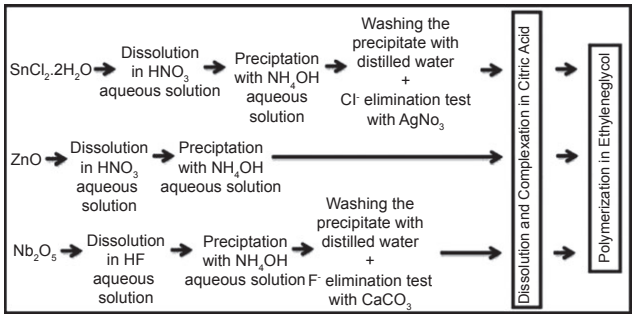

Fig. 1. Block scheme for preparation of the polymeric solution by Pechini Method.

complex organic matrix and decreases the segregation of metals during calcination of the polymeric resin. The used processing allows the addition of many modifiers in small amount giving its homogenous distribution in the ceramic matrix. The molar ratio of metal:citric acid: ethylene glycol for Sn^{4+} solution was 1:3:6 and for Zn^{2+}, Nb^{5+} solutions was 1:4:16.

The polymeric resin of interest was obtained by mixing 98.95 mol% of SnO_2, 1 mol% of ZnO and 0.05 mol% of Nb_2O_5 and it was obtained: $(0.9895)SnO_2(0.01)ZnO(0.0005)Nb_2O_5$. The ceramic powder was obtained by controlled calcination of the resin (350°C/1 h, followed by 500°C/2 h—heating rate of 5°C/min) until the complete formation of oxides. The material was then milled in order to break the agglomerate of particles. The calcination of polymeric solution, followed by milling, also provides a nanopowder with spherical morphology and size distribution resulting in high surface area (57 m^2/g).[19,20]

(3) Electrophoretic Deposition

The deposition of (Zn, Nb)-SnO_2 nanoparticles on Si/Pt substrate [Si(100)/TiO_2(1 μm)/Ti (20 nm)/Pt (150 nm)] by electrophoretic deposition technique (EPD)[21–23] was used to obtain the ceramics film, providing a rapid deposition and uniform thickness.

NdFeB magnets of 11 mm × 1.5 mm circular shape and with Ni surface treatment and were coupled to the electrodes in a system containing ethylic suspension (7 mg of powder in 20 mL of alcohol) and 0.02 g of solid iodine to increase the surface charge, as shown in Fig. 2. These modifications were carried out to improve the ionization process of the particles from the alignment of the dipole orientation and thus increase the deposition rate.

A voltage of 2 kV for 10 min was applied in the system using a high voltage source—Hipot ET 5000cc Serta (ElectricTest Serta, Belo Horizonte/MG, Brazil) with a current of approximately 2.0 mA. The addition of iodine and magnets were needed to increase the deposition rate of the particles and density of the film, thereby decreasing the presence of pores. After deposition, the films obtained were submitted for heat treatment at 250°C/30 min for iodine evaporation.

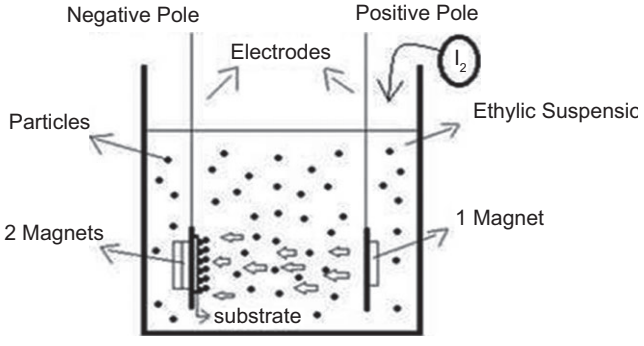

Fig. 2. Electrophoretic deposition system developed by the authors.

(4) Microwave Sintering

The use of microwave oven for sintering has advantages such as the use of a shorter sintering time, high heating rates, better control of sintering due to minimize the diffusion of metal electrode of the substrate into the material and enhances the mass diffusion by vibrational and rotational motions of molecules.[24]

The sintering of the films occurred in a microwave oven of 770 W and frequency of 2.45 GHz, adapted by the research group itself with a temperature controller. The sintering was carried out at 1000°C for 40 min, which promoted considerable reduction in pores and the formation of necks between grains.

(5) Addition of Cr^{3+} and Heat Treatment

A thin layer of Cr^{3+} ions was also deposited by electrophoresis on the surface of the sintered films. The films were immersed in a cell containing 0.3 mol/L of chromium solution and a voltage of 2 kV for 5 min was applied in the system. Then, each sample was thermally treated in a microwave oven to promote the diffusion of Cr^{3+} in the grains. A sample without Cr^{3+} was prepared (Film 0) to check the action effect of chromium surface deposition on the potential barrier. Table I shows details of the temperature and time of heat treatment used for the diffusion of Cr^{3+} ions. To verify the reproducibility of the technique applied on the electrical properties of ceramic films, more than one sample were prepared at same conditions for diffusion of chromium: 1000°C/10 min (Film 5, Film 5.1 and Film 5.2) and 1000°C/15 min (Film 6, Film 6.2 and Film 6.1).

(6) Characterization

Thermal analysis was carried out using thermo-gravimetric analysis. Netzsch-Thermische (Selb, Germany) Analyse PU 1.851.01 and TASC (Selb) 414/2 controller. Alpha alumina (α-Al_2O_3) was used as standard. The equipment was operated at a constant heating step of 10°C/min in an air atmosphere of 30 cm^3/min. The thermal analysis was carried out up to 650°C. Technique of adsorption–desorption of N_2 gas in the samples (BET method) carried out by ASAP 2010 (Micromeritics, Norcross, GA) equipment was used to measure the surface area of the powder.

XRD measurements were carried out at Rigaku (Tokyo, Japan) equipment RINT2000 model. The experimental conditions were as follows: range of 20°–80° with increment of $\Delta 2\theta = 0.02°$ and copper radiation (40 kV, 20 mA). The XRD pattern for SnO_2-based system obtained was analyzed and compared with JCPDS-ICDD card (no. 41-1445). SEM images were obtained by JEOL (Peabody, MA) 7500F model-field emission scanning microscope, to provide a qualitative morphological analysis of the sintered samples (grains and pores).

(7) Electrical Measurements

The effect of the addition and diffusion of Cr^{3+} on the electronic conductivity in conjunction with the formation of potential barrier was verified by the studies of current-voltage

Table I. Heat Treatment Conditions after Cr^{3+} Deposition by EPD on the Sintered Film Surface

Sample	Heat treatment	Sample	Heat treatment
Film 0	(without Cr^{3+})	Film 4	1000°C/5 min
Film 1	900°C/5 min	Film 5, Film 5.1, Film 5.2	1000°C/10 min
Film 2	900°C/10 min	Film 6, Film 6.1, Film 6.2	1000°C/15 min
Film 3	900°C/15 min		

analysis as a function of temperature. The measurements were performed in air at room temperature and in the range of 50°C–300°C with intervals of 50°C and stabilization of temperature for 20 min.

By the DC Sputtering technique, the platinum top electrodes were deposited on the film's surface using a mask with circular holes with a diameter of 300 μm, and then electrical measurement was carried out in the transverse section in the samples (platinum from the substrate acts as the bottom electrode). The value of nonlinear coefficient is determined by Eq. (8), derived from Eq. (5). The calculation of α relative to the electric field (E) and current density (J) is defined in Eqs. (6) and (7).

$$\alpha = \frac{\log J_2 - \log J_1}{\log E_2 - \log E_2} \tag{5}$$

Values of the electric field and current density are obtained from the equations:

$$E = V/d \tag{6}$$

$$J = I/A \tag{7}$$

where d represents the sample thickness and A the area of the electrode deposited on the surface of the film. For the calculation of α, the range of 1–10 mA/cm^2 current density was used, i.e., $J_1 = 1$ and $J_2 = 10$, then:

$$\alpha = (\log E_2 - \log E_1)^{-1} \tag{8}$$

The breakdown electric field (E_R) is equivalent to the field when the current density is 1 mA/cm² (J_1). To evaluate the electronic resistivity on the grain boundary of the samples (ρ_{GB}), an analysis was performed in the linear region of low current (0 mA/cm² at 1 mA/cm²) of E versus J curves as function of temperature. The resistivity was determined by the slope of the line obtained by linear regression in the ohmic region. Pianaro et al.[25] studied SnO_2-based ceramics and determined the conduction as being the Schottky type, where the conduction occurs through the potential barrier formed in the grain-boundary region through the action of the electric field and the temperature. The equation that describes this behavior is as follows:[26–28]

$$J_S = A^* \cdot T_2 \cdot \exp\left[-\frac{\phi_b \beta E_{1/2}}{kT}\right] \tag{9}$$

where A^* is Richardson constant, ϕ_b represents the height of the potential barrier, E is the electrical field, T is ambient temperature in Kelvin and β a constant related to the width of the potential barrier, according to the equation:

$$\beta = (d\omega)^{-1/2} \tag{10}$$

where d representing the average grain size and ω the width of the barrier.

III. Results and Discussion

The XRD analysis of SnO_2-based powder was carried out previously by the authors.[29] It was shown that SnO_2-rutile phase was formed (JCDPS no 41-1445) and no secondary phase formation was noticed.

For deposition by electrophoresis, an ethylic alcohol suspension formed by SnO_2-based powder was used in a system as showed in Fig. 2 [and described in Section II(3)]. The films obtained were sintered in a microwave oven at 1000°C/40 min, further returned to EPD system for the deposition of Cr^{3+} ions on surface of the films and then different heat treatments in a microwave oven were applied, according to Table I. The steps were schematized in the flow diagram:

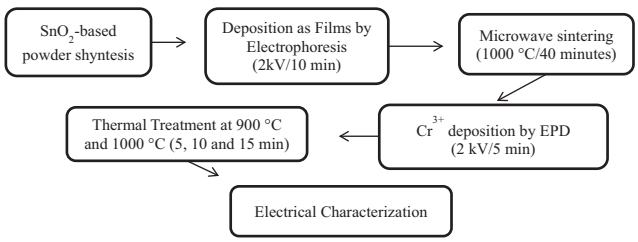

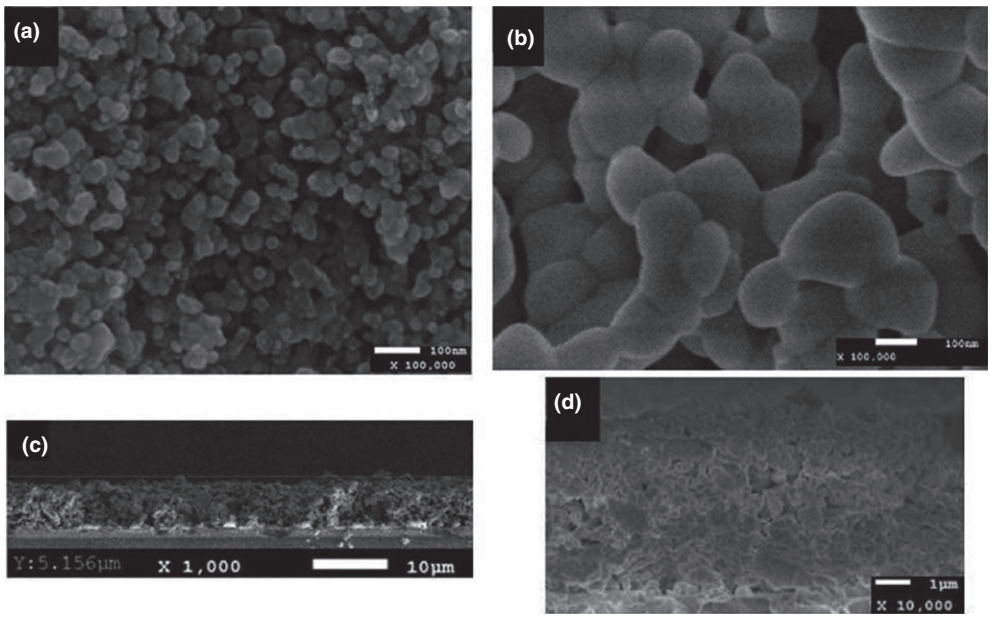

Fig. 3. SEM of (Zn, Nb)-doped SnO_2: (a) particles after synthesis process; (b) top vision of the film sintered at 1000°C/40 min in a microwave oven; (c) and (d) cross sections of the sintered films (different magnifications).

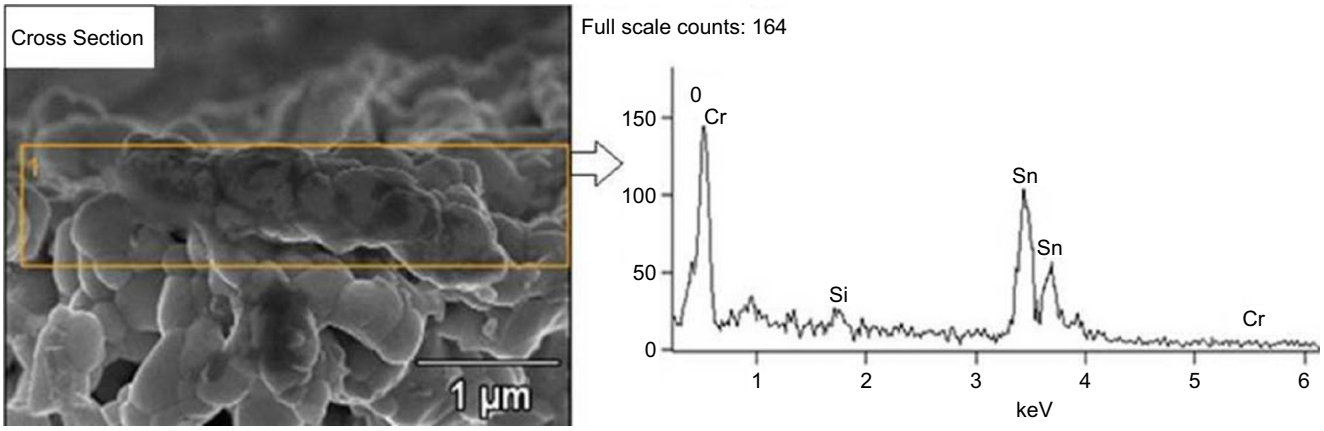

Fig. 4. EDS of sintered film after Cr^{3+} deposition by EPD and thermally treatment at 1000°C/15 min in a microwave oven.

Table II. Values Calculated for the Coefficient of Nonlinearity (α), Breakdown Electric Field (E_R) and Breakdown Voltage (V_R) for Films Sintered at 1000°C/40 min Without and with Cr^{3+} [29]

Sample	Heat treatment	α	E_R (kV/cm)	V_R (Volts)	I_F (A)
Film 0	Without Cr^{3+}	1.7	5.0	2.5	6.8×10^{-4}
Film 1	900°C/5 min	4.2	22.0	11.0	5.4×10^{-4}
Film 2	900°C/10 min	5.8	128.0	64.0	6.7×10^{-4}
Film 3	900°C/15 min	7.2	130.0	64.5	2.8×10^{-4}
Film 4	1000°C/5 min	9.6	48.0	24.0	4.6×10^{-4}
Film 5	1000°C/10 min	10.3	125.0	62.5	4.4×10^{-5}
Film 5.1	1000°C/10 min	10.5	141.0	70.4	6.2×10^{-6}
Film 5.2	1000°C/10 min	10.8	157.0	78.5	1.6×10^{-6}
Film 6	1000°C/15 min	11.4	119.0	59.5	4.8×10^{-6}
Film 6.1	1000°C/15 min	13.8	151.0	75.5	8.5×10^{-6}
Film 6.2	1000°C/15 min	11.5	120.0	60.4	2.8×10^{-6}

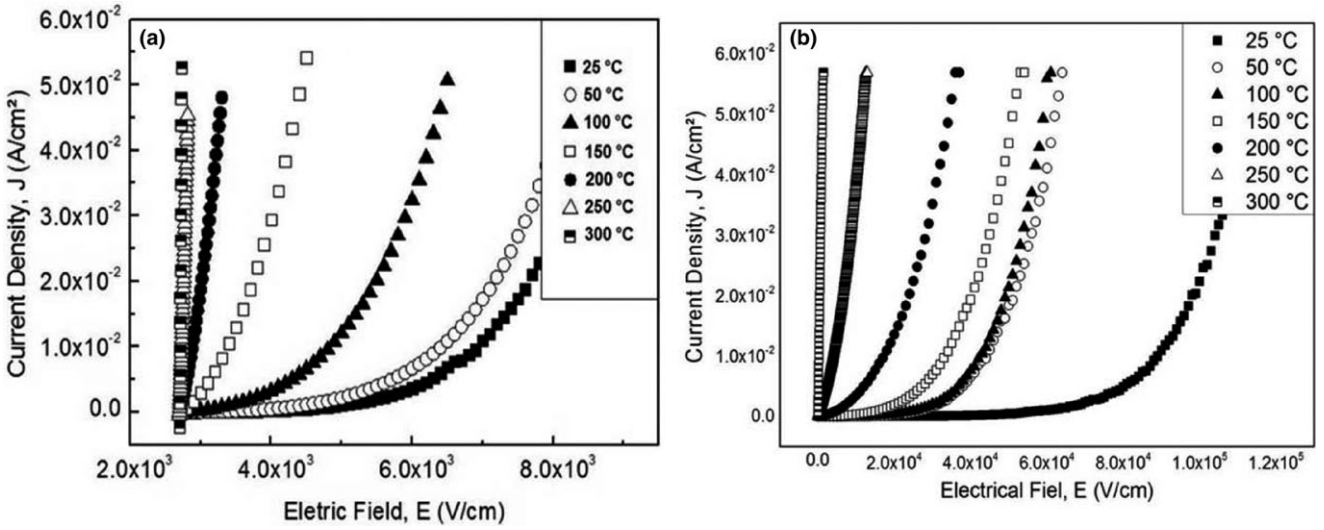

Fig. 5. *E* versus *J* curves as a function of temperature (a) for film without deposition of chromium and (b) for film thermal treated at 900°C/15 min after Cr^{3+} deposition.

By using the ImageJ software to analyze the SEM images, it was possible to verify that the synthesis methodology allowed obtaining nano-sized particles [Fig. 3(a)] with an average diameter of 20 nm and after deposition of the particles as film and microwave sintering, the particles [Fig. 3(b)] had an average diameter of 190 nm. According to the cross section image [Figs. 3(c)–(d)], the films possess homogeneous thickness of 5 µm. The EDS analysis presented in Fig. 4 shows that Zn and Nb were uniformly distributed in the solid solution of SnO_2-powder and no evidence of their segregation and no presence of any other ion as contaminants was noticed. That confirms that Cr^{3+} ions deposited by EPD were well done.

The films were previously characterized according to.[29] The current-voltage analysis (*I* versus *V*) for evaluation of nonlinear coefficient and breakdown voltage indicated that the films had improved varistor behavior after thermal treatment in a microwave oven due to Cr^{3+} diffusion,

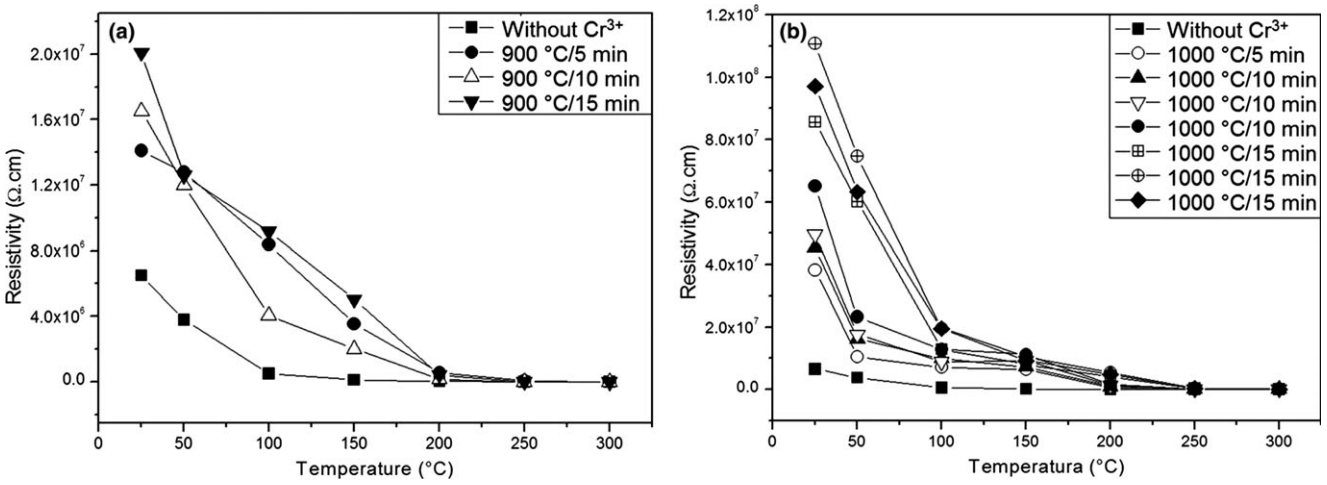

Fig. 6. Curves of resistivity (ρ) for the films submitted to *I* versus *V* analysis as a function of temperature (after thermal treatment for Cr^{3+} deposition).

without change in the SnO_2-microstructure. The increase in the nonlinear coefficient and breakdown voltage caused by the addition and diffusion of Cr^{3+} was present in Table II. All films were modified with chromium that showed a varistor nominal voltage (the breakdown voltage at current density of 1 mA) within the range of a commercial varistor.[30]

Table III. Values Calculated After Analysis *I* versus *V* a Function of Temperature

Sample	Heat treatment	10^7 ρ_{GB} (Ω.cm)†	ϕ_b(eV)	ω/ω_{max}‡
Film 0	Without Cr3+	0.6	0.34	0.97
Film 1	900°C/5 min	1.4	0.51	1.00
Film 2	900°C/10 min	1.7	0.56	0.38
Film 3	900°C/15 min	2.1	0.64	0.24
Film 4	1000°C/5 min	3.8	0.47	0.67
Film 5	1000°C/10 min	4.5	0.56	0.57
Film 5.1	1000°C/10 min	4.9	0.58	0.54
Film 5.2	1000°C/10 min	6.5	0.60	0.59
Film 6	1000°C/15 min	8.6	0.61	0.21
Film 6.1	1000°C/15 min	11.1	0.68	0.29
Film 6.2	1000°C/15 min	9.7	0.60	0.24

†Values of ρGB determinate at 25°C.

‡This value is used to check how much the width (ω) decreased compared to the sample with greater width of the potential barrier ($\omega_{Film1} = \omega_{max}$).

The improvement of nonlinear coefficient was caused by better distribution of chromium at grain boundaries that results in longer heat treatment time, leading to the creation of higher potential barriers due to increase in concentration of electron donors' species. Thus, the deposition of particles by electrophoresis, microwave oven sintering, and Cr^{3+} diffusion after thermal treatment can produce films with good reproducibility (Films 5.1, 5.2, 6.1, and 6.2) looking for low-voltage varistors characteristics.

To verify the electrical conduction in a grain-boundary region due to formation of the potential barrier, all the films were *I* versus *V* characterized as a function of temperature. Figure 5(a) shows *E* versus *J* graph for Film 0 measured at different temperature. The films thermally treated after deposition of Cr^{3+} [Fig. 5(b)] exhibited a similar behavior as Film 0 with curves of non-ohmic behavior until 100°C. It can be observed that an increase in temperature led to an increase in electrical conduction, thus characterizing the electrical conduction of the thermionic type.

The resistivity was determined from the slope obtained by linear regression in the ohmic region (low current region of 0 mA/cm² at 1 mA/cm²) from curves presented in Fig. 5. The

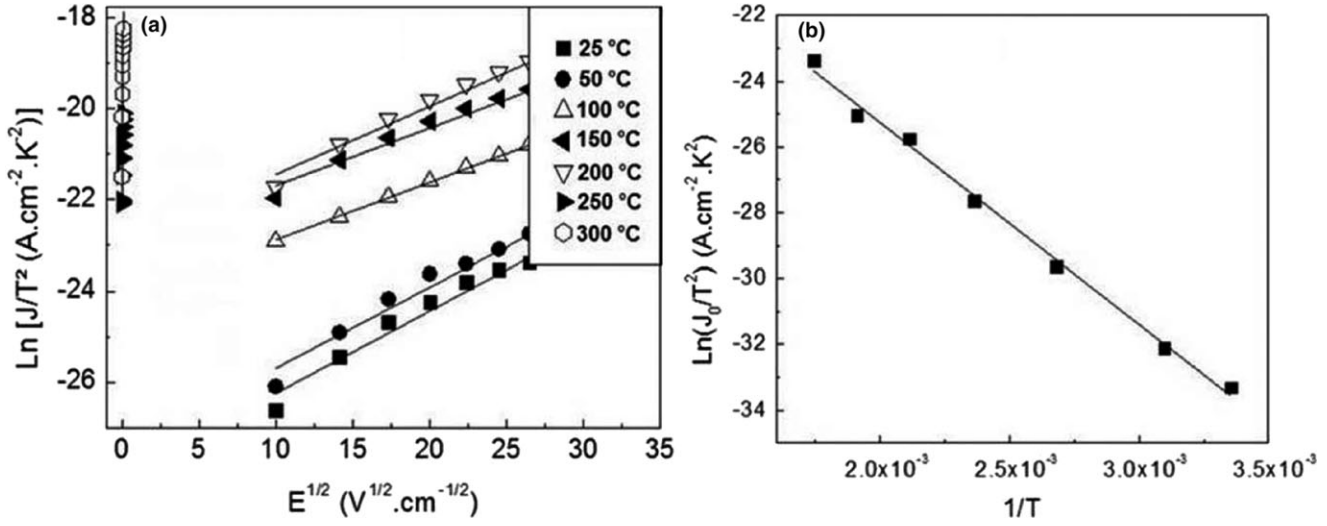

Fig. 7. (a) Curves $\mathrm{Ln}(J/T^2)$ versus $E^{1/2}$ for Film 0 analyzed at different temperatures. (b) Linear fit of Ln (J_0/T^2) from extrapolation to $E = 0$ of curves of (a).

behavior of the resistivity at different temperatures is shown in Fig. 6, making it possible to observe a significant variation between 25°C and 100°C.

It was noticed that the films thermally treated at 1000°C after deposition of Cr^{3+} [Fig. 6(b)] possessed highest resistivity than films treated at 900°C [Fig. 6(a)]. This can be associated with chromium diffusion rate, which was higher with increase in temperature of thermal treatment, and influences on generation of defects on the grain boundaries. The defects such as oxygen vacancies, which contribute to an increase in the height of the potential barrier, leading to a higher block of electrical current, and consequently increasing the resistivity values. Also, it was indicated that the samples prepared from the same batch showed similar values, confirming the efficiency of the applied technical reproducibility onto electrical properties. All films with Cr^{3+} showed higher resistivity compared to the film without Cr^{3+} (Table III). All samples possess similar values of resistivity over 100°C, due to the effect of temperature that activates the electronic conduction process.

From the data collected by I versus V analysis as a function of temperature [Fig. 5(a)] were plotted curves $\mathrm{Ln}(J/T^2)$ versus $E^{1/2}$ [Fig. 7(a)]. By extrapolation $E = 0$, the values of $\mathrm{Ln}(J_0/T^2)$ were obtained from the intersection of the curves with the Y axis and plotted graphs of $\mathrm{Ln}(J_0/T^2)$ versus $1/T$ [Fig. 7(b)]. For each sample, the height (ϕ_b) of the potential barrier formed in the grain boundary was calculated from the slope of the curve of Fig. 7(b) and the value of β was determined from the curve at 25°C of Fig. 7(a), and then the width (ω) of the potential barrier was calculated from Eq. (10) (Table III)

It was observed that the addition and diffusion of Cr^{3+} ions on the surface of the film caused significant modification in the potential barrier that increased by increasing the temperature of the thermal treatment. The values of resistivity on grain boundary (ρ_{GB}) increase significantly. The highest value of resistivity was obtained for Film 6 and was attributed to the highest potential barrier. The increase in the potential barrier height (ϕ_b) will decrease the transport of electric current, thereby improving the nonlinearity coefficient (Table II). The increase of ϕ_b and decrease of ω suggest that the addition of Cr^{3+} causes modification on the potential barrier by increasing the density of the electronic charges in the grain boundary.

IV. Conclusions

The application of Cr^{3+} results in the modification of the potential barrier and resistivity, compared to the sample without Cr^{3+} superficial addition. Furthermore, an increase in the potential barrier leads to an improvement to block the electrical current into the material, resulting in an increase in the varistors properties (nonlinear coefficient, resistivity). This effect occurs due to the increase in concentration of electron donors species in the grain boundary.

The applied methodology allowed obtaining a ceramic powder with homogeneous composition, particles with spherical morphology and uniform size distribution. Using microwave sintering at 1000°C for 40 min and EPD was possible to obtain films with homogeneous thickness (5 μm) and varistors properties with a relatively high nonlinear coefficient of 9–14 and breakdown voltage below 80 V, further improvement of properties prospectively will allow their application as low voltage varistors, replacing the commercial ZnO varistors.

Acknowledgments

The authors thank the LMA-IQ for providing the FEG-SEM facilities, and the financial support of this research project by the Brazilian research funding agencies CNPq and CEPID/CDMF-FAPESP 2013/07296-2.

References

[1]L. Perazolli, et al., "Structural and Microstructural Behavior of SnO_2 Dense Ceramics Doped with ZnO and WO_3," *Mater. Lett.*, **59** [14–15] 1859–65 (2005).

[2]M. Cilense, et al., "Effect of Seed Addition on SnO_2-Based Varistor for Low Voltage Application," *J. Am. Ceram. Soc.*, **96** [2] 524–30 (2013).

[3]J. A. Aguilar-Martínez, M. I. PechCanul, M. B. Hernándes, A. B. Glot, E. Rodríguez, and L. G. Ortiz, "Effect of Sintering Temperature on the Electric Properties and Microstructure on SnO_2-Co_3O_4-Sb_2O_5-Cr_2O_3 Varistor Ceramic," *Ceram. Int.*, **39** [4] 4407–12 (2013).

[4]D. R. Clarke, "Varistor Ceramics," *J. Am. Ceram. Soc.*, **82**, 485–502 (1999).

[5]J. He, Z. Peng, Z. Fu, C. Wang, and X. Fu, "Effect of ZnO Doping on Microstructural and Electrical Properties of SnO_2-Ta_2O_5 Based Varistors," *J. Alloy. Compd.*, **528** [5] 79–83 (2012).

[6]C. M. Wang, J. F. Wang, and W. B. Su, "Microstructural Morphology and Electrical Properties of Copper- and Niobium-Doped Tin Dioxide Polycrystalline Varistors," *J. Am. Ceram. Soc.*, **89** [8] 2502–8 (2006).

[7]S. P. Jiang, J. G. Love, and S. P. S. Badwal, "Electrochemical Techniques in Studies of Solid Ionic Conductors," *Key Eng. Mater.*, **125–126**, 81–132 (1996).

[8]K. S. Kirkpatrick, T. O. Mason, U. Balachandran, and R. B. Poeppel, "Impedance Spectroscopy Study of Sintering in Bi-Doped ZnO," *J. Am. Ceram. Soc.*, **77** [6] 1493–8 (1994).

[9]A. B. Glot, A. V. Gaponov, and A. P. Sandoval-García, "Electrical Conduction in SnO_2 Varistors," *Phys. B*, **405** [2] 705–11 (2010).

[10]H. Bastami and E. Taheri-Nassaj, "(Co, Nb, Sm)-Doped Tin Dioxide Varistor Ceramics Sintered Using Nanopowders Prepared by Coprecipitation Method," *J. Am. Ceram. Soc.*, **94** [10] 3249–55 (2011).

[11]J. A. Aguilar-Martínez, M. I. Pech-Canul, M. B. Hernández, A. B. Glot, E. Rodrígez, and L. Gracía Ortiz, "Effect of Cr_2O_3 on the Microstructure and Non-Ohmic Properties of (Co, Sb)-Doped SnO_2 Varistor," *Rev. Mex. Fis.*, **59** [1] 6–9 (2013).

[12]R. Leite, W. C. Las, M. A. Zaghete, M. Cilense, and J. A. Varela, "The Effect of Cr Concentration and Preparation Method on the Microstructure and Electrical Characterization of SnO_2-Based Ceramics," *Mater. Res.*, **6** [4] 457–61 (2003).

[13]C. P. Li, et al., "Nonlinear Electrical Properties of Cobalt Doped SnO_2·Ni_2O_3·Nb_2O_5 Varistors," *Eur. Phys. J-Appl. Phys.*, **16** [1] 3–9 (1997).

[14]M. O. Orlandi, P. R. Bueno, E. R. Leite, and E. Longo, "Non-Ohmic Behavior of SnO_2·MnO_2-Based Ceramics," *Mater. Res.*, **6** [2] 279–83 (2003).

[15]F. M. Filho, A. Z. Simões, A. Ries, L. Perazolli, E. Longo, and J. A. Varela, "Dependence of the Nonlinear Electrical Behavior of SnO_2-Based Varistors on Cr_2O_3 Addition," *Ceram. Int.*, **33** [2] 187–92 (2007).

[16]W. X. Wang, J. F. Wang, H. C. Chen, W. B. Su, and G. Z. Zang, "Effects of Cr_2O_3 on the Properties of (Co, Nb)-Doped SnO_2 Varistors," *Mat. Sci. Eng. B*, **99** [13] 470–4 (2003).

[17]Q. Wei, J. He, J. Hu, and Y. Wang, "Influence of Cr_2O_3 on the Residual Voltage Ratio of SnO_2-Based Varistor," *Cerâmica, J. Am. Ceram. Soc.*, **94** [7] 1999–2002 (2011).

[18]P. R. Bueno, S. A. Pianaro, E. C. Pereira, L. O. S. Bulhões, E. Longo, and J. A. Varela, "Investigation of the Electrical Properties of SnO_2 Varistor System Using Impedance Spectroscopy," *J. Appl. Phys.*, **84** [7] 3700–5 (1998).

[19]M. P. Pechini, "Method of Preparing Lead and Alkaline Titanates and Niobates and Coating Method Using the Same to Form a Capacitor"; U.S. Patent no. 3330697. 1967.

[20]B. D. Stojanovic, V. Mitic, V. Pejovic, M. M. Vijatovic, and M. A. Zaghete, "Screen Printed PLZT Thick Films Prepared from Nanopowders," *J. Eur. Ceram. Soc.*, **27** [13–15] 4359–62 (2007).

[21]F. Q. Tang, T. Uchikoshi, and Y. Sakka, "Electrophoretic Deposition Behavior of Aqueous Nanosized Zinc Oxide Suspensions," *J. Am. Ceram. Soc.*, **85** [9] 2161–5 (2002).

[22]I. Corni, M. P. Ryan, and A. E. Boccaccini, "Electrophoretic Deposition: From Traditional Ceramics to Nanotechnology," *J. Eur. Ceram. Soc.*, **28** [7] 1353–67 (2008).

[23]O. Van der Biest, S. Put, G. Anné, and J. Vleugels, "Electrophoretic Deposition for Coatings and Free Standing Objects," *J. Mater. Sci.*, **39** [3] 779–85 (2004).

[24]R. R. Menezes, P. M. Souto, and R. H. G. A. Kiminami, "Sinterização de Cerâmicas em Microondas. Part I: Aspectos Fundamentais," *Cerâmica*, **53** [325] 1–10 (2007).

[25]S. A. Pianaro, P. R. Bueno, P. Olivi, E. Longo, and J. A. Varela, "Electrical Properties of the SnO_2-Based Varistor," *J. Mater. Sci.-Mater. El.*, **9**, 159–65 (1998).

[26]T. K. Gupta, "Application of Zinc Oxide Varistors," *J. Am. Ceram. Soc.*, **73** [7] 1817–40 (1990).

[27]J. F. Wang, W. B. Su, H. C. Chen, W. X. Wang, and G. Z. Zang, "(Pr, Co, Nb)-Doped SnO_2 Varistors Ceramics," *J. Am. Ceram. Soc.*, **88** [2] 331–4 (2005).

[28]A. A. Felix, M. O. Orlandi, and J. A. Varela, "Schottky-Type Grain Boundaries in CCTO Ceramics," *Solid State Commun.*, **151** [19] 1377–81 (2011).

[29]G. M. M. M. Lustosa, J. P. C. Costa, L. A. Perazolli, B. D. Stojanovic, and M. A. Zaghete, "Electrophoretic Deposition of (Zn, Nb)SnO_2-Films Varistor Superficially Modified with Cr^{3+}," *J. Eur. Ceram. Soc.*, **35** [7] 2083–9 (2015).

[30]Littelfuse. AUMOV™ & LV UltraMOV™ Varistor Design Guide for DC & Automotive Applications. 2015, http://www.littelfuse.com/~/media/electronics/design_guides/varistors/littelfuse_varistor_dc_application_varistor_design_guide.pdf.pdf (accessed 1 July 2015). □